Site-directed mutagenesis and stability of the carboxylic acid reductase MAB4714 from Mycobacterium abscessus

Fedorchuk, Tatiana P.; Khusnutdinova, Anna N.; Flick, Robert; Yakunin, Alexander

Journal of Biotechnology

DOI:
10.1016/j.jbiotec.2019.07.009

Published: 10/09/2019

Peer reviewed version

Title: Site-directed mutagenesis and stability of the carboxylic acid reductase MAB4714 from *Mycobacterium abscessus*

Authors: Tatiana P. Fedorchuk, Anna N. Khusnutdinova, Robert Flick, Alexander F. Yakunin

PII: S0168-1656(19)30807-7
DOI: https://doi.org/10.1016/j.jbiotec.2019.07.009
Reference: BIOTEC 8477

To appear in: *Journal of Biotechnology*

Received date: 15 June 2019
Revised date: 24 July 2019
Accepted date: 25 July 2019

Please cite this article as: Fedorchuk TP, Khusnutdinova AN, Flick R, Yakunin AF, Site-directed mutagenesis and stability of the carboxylic acid reductase MAB4714 from *Mycobacterium abscessus*, *Journal of Biotechnology* (2019), https://doi.org/10.1016/j.jbiotec.2019.07.009

Site-directed mutagenesis and stability of the carboxylic acid reductase MAB4714 from *Mycobacterium abscessus*

Tatiana P. Fedorchuk[1,2], Anna N. Khusnutdinova[1,2], Robert Flick[1], and Alexander F. Yakunin[1,3*]

[1] Department of Chemical Engineering and Applied Chemistry, University of Toronto, Toronto, Ontario, M5S 3E5, Canada

[2] Institute of Basic Biological Problems, Russian Academy of Sciences, Pushchino, Moscow region, 142290, Russia

[3] Centre for Environmental Biotechnology, School of Natural Sciences, Bangor University, Gwynedd LL57 2UW, UK

[*] Corresponding author (a.iakounine@utoronto.ca; a.iakounine@bangor.ac.uk)

Highlights

- Structural modeling of carboxylic acid reductase (CAR) MAB4714 revealed the residues of its carboxylate-binding pocket.
- Succinate reductase activity of MAB4714 was increased by over 2-fold by mutating Leu284 or Thr285 to Trp.
- The conserved Ser residue of the CAR phosphopantheteine attachment site is critical for protein stability in solution.

Abstract

Carboxylic acid reductases (CARs) catalyze ATP- and NADPH-dependent reduction of carboxylic acids to corresponding aldehydes. Although successful applications of these enzymes for the bioconversion of monocarboxylic acids have already been reported, their applicability for the reduction of dicarboxylic acids is not well understood. Here, we explored the possibility of engineering CARs for enhanced activity toward succinic acid for potential applications in 1,4-butanediol production. Structural models of the carboxylate-binding pocket of the CAR enzyme MAB4714 from *Mycobacterium abscessus* suggested that its reactivity toward succinic acid could be enhanced by reducing the pocket volume. Using site-directed mutagenesis, we introduced larger side chains into the MAB4714 carboxylate binding pocket and compared the activity of 16 mutant proteins against cinnamic and succinic acids. These experiments revealed that, although the reaction rates remain low, the replacement of Leu284 or Thr285 with Trp

increased activity toward succinic acid more than two times. The T285E mutant protein also showed increased activity toward succinic acid, but it was lower than that of T285W. The mutated residues of MAB4714 are located on the flexible loop covering the carboxylate-binding pocket, which appears to contribute to substrate preference of CARs. Thus, reductase activity of CARs against succinic acid can be improved by introducing large side chains into the carboxylate-binding pocket. We also discovered that alanine replacement of the conserved Ser713 in the CAR phosphopantetheine attachment site resulted in complete degradation of the full-length protein into separate A and R domains, suggesting that CAR phosphopantetheinylation is important for its stability in solution.

Keywords

Carboxylic acid reductase, succinic acid reduction, site-directed mutagenesis, protein stability, *Mycobacterium abscessus*

1. Introduction

Carboxylic acids serve as precursors for a broad range of commodity chemicals and polymers. Their importance for the chemical industry has been underlined in the US DoE list of the top 12 platform chemicals, which includes nine organic acids (Bozell, 2010; Jang et al., 2012). Many carboxylic acids are available in great abundance as renewable feedstocks including succinic acid, citric acid, and ferulic acid (Napora-Wijata et al., 2014). Bio-based production of organic acids has become a rapidly growing field due to recent advances in metabolic engineering and synthetic biology (Alonso et al., 2015; Bornscheuer et al., 2012). Increasing production of carboxylic acids from renewable resources makes them attractive precursors for a broad range of valuable products such as polymers, aldehydes, and alcohols. However, chemical reduction of carboxylic acids to aldehydes is an energetically demanding reaction, which is also difficult to control because of the low energy barrier for the further reduction to an alcohol. Although many advances in chemocatalytic reduction have been reported, these methods usually depend on activated carboxylates, require harsh reaction conditions, and produce considerable amounts of toxic waste. Biocatalytic reduction of carboxylic acids offers the typical advantages of enzyme-catalyzed processes, including chemoselectivity, enantioselectivity, and mild reaction conditions (Hollmann, 2011; Napora-Wijata et al., 2014). Therefore, biocatalytic reduction of organic acids is gaining importance.

Currently, several biological routes to carboxylic acid reduction are known including direct reduction, catalyzed by a single enzyme or two-enzyme cascades with thioester or phosphoester intermediates (Kramer et al., 2018; Napora-Wijata et al., 2014). Carboxylate reductases (CARs, EC 1.2.1.30) from aerobic organisms (bacteria, fungi,

plants) catalyze the reduction of a carboxylate substrate to the corresponding aldehyde using ATP and NADPH as cofactors (Gross, 1969; Li and Rosazza, 1997). In the first step, these enzymes catalyze the initial reaction between a carboxylic acid and ATP producing an acyl-AMP intermediate, which is then reduced by NADPH to form the aldehyde product. Biochemical studies with the purified CAR from *Nocardia iowensis* demonstrated a large protein (over 1,000 residues) with three domains: an N-terminal adenylation (A) domain, a C-terminal reductase (R) domain with a phosphopantetheine attachment site, and a trans-thiolation domain (T), also called PCP, peptidyl carrier protein located between them (He et al., 2004; Li and Rosazza, 1998; Venkitasubramanian et al., 2007). For maximal activity, the recombinant *N. iowensis* CAR required post-translational phosphopantetheinylation at a conserved Ser residue in the T-domain by a phosphopantetheinyl transferase (added as a purified protein or co-expressed in *E. coli*) (Venkitasubramanian et al., 2007). The detailed mechanism of the CAR reaction cascade from acid to aldehyde is not fully understood (Winkler, 2018). The proposed catalytic model of CAR reaction suggests that the deprotonated acid is activated by ATP at the A-domain producing an acyl-AMP intermediate, which is nucleophilically attacked by the phosphopantetheine thiol, with the formation of covalently bound acyl thioester and AMP (He et al., 2004; Venkitasubramanian et al., 2007; Winkler, 2018). The acyl thioester-phosphopantetheine moiety then moves from the A-domain to the R-domain, where the acyl thioester is reduced by NADPH producing a free aldehyde and enzyme. The recent determination of crystal structures for individual domains and their combinations (A-T and T-R) of three CARs from *Segniliparus rugosus* (*Sr*CAR), *Nocardia iowensis* (*Ni*CAR), and *Mycobacterium marinum* (*Mm*CAR) represents a major

breakthrough in our understanding of the molecular mechanisms of CAR activity and substrate selectivity (Gahloth et al., 2017). The structures of CARs revealed large-scale domain motions during the reaction, and suggested that molecular interactions between the A and R domains are limited to competing T-docking sites. These studies also identified the presence of a mobile C-terminal sub-domain in the A domain of bacterial CARs which adopts distinct positions(Gahloth et al., 2017). Structure-based site-directed mutagenesis of CARs from *S. rugosus* and *Neurospora crassa* identified several residues critical for catalytic activity of these enzymes (Gahloth et al., 2017; Stolterfoht et al., 2018).

Purified CARs from different organisms have been shown to accept a broad range of carboxylic acids as substrates with some enzymes being more promiscuous than others (Akhtar et al., 2013; Finnigan et al., 2017; Khusnutdinova et al., 2017; Li and Rosazza, 1997; Napora-Wijata et al., 2014; Winkler, 2018). A recent detailed kinetic analysis of CARs suggested that substrate preference of these enzymes is determined by the first step in the proposed reaction mechanism (formation of acyl-AMP intermediate), which is an ordered sequential Bi Bi reaction with ATP bound before the carboxylate substrate (Finnigan et al., 2017). The substrate profiles of characterized CARs largely overlap and include aromatic, heteroaromatic, and aliphatic (from C2 to C18) carboxylic acids, as well as bifunctional carboxylic acids (diacids, hydroxyacids, oxoacids, and amino acids) (Khusnutdinova et al., 2017; Kramer et al., 2018). With monocarboxylic acids as substrates, purified CARs exhibited significant reductase activity toward C3-C16 substrates with maximal activity against C4-C12 acids (Akhtar et al., 2013; Khusnutdinova et al., 2017). However, their activity was diminished toward substrates

containing additional polar or charged groups (hydroxy, oxo, carboxy, or amino) (Khusnutdinova et al., 2017; Kramer et al., 2018). Nevertheless, CARs can tolerate the presence of a second charged or polar group in their substrates.

The broad substrate scope and kinetic characteristics of CARs suggest the potential for their application as industrial biocatalysts (Finnigan et al., 2017; Winkler, 2018). Several successful applications of CARs have already been demonstrated for the microbial production of alkanes, propane, and aromatic aldehydes (Akhtar et al., 2013; Kallio et al., 2014; Kunjapur et al., 2014; Schwendenwein et al., 2016; Sheppard et al., 2016; Sheppard et al., 2014). Interestingly, *Mav*CAR from *Mycobacterium avium* and *Mar*CAR from *Mycobacterium aromaticivorans* have been shown to be active towards both succinic and lactic acid, which are central microbial metabolites (Kramer et al., 2018). Succinic acid can be biocatalytically transformed to 1,4-butanediol (1,4-BDO) using the heterologous biosynthetic pathway established in *E. coli* by Genomatica (Fig.1) (Yim et al., 2011). 1,4-BDO is an important non-natural chemical, which is used as a precursor for the synthesis of different polymers. The reported 1,4-BDO pathway (from succinate to 1,4-BDO) includes six enzymes, and produces 4-hydroxybutyrate as an intermediate (Yim et al., 2011). Recently, we demonstrated that several CARs including MAB4714 from *Mycobacterium abscessus* exhibit significant reductase activity toward 4-hydroxybutyrate, producing 4-hydroxybutanal as the product (Khusnutdinova et al., 2017). Using various combinations of CARs and aldo-keto reductases, we observed up to 95% conversion of 4-hydroxybutyrate to 1,4-BDO (Khusnutdinova et al., 2017), suggesting that the reported 1,4-BDO pathway can be shortened to five enzymes using CARs (Fig. 1). Moreover, structural studies of CARs reported that these enzymes can be

engineered to catalyze two sequential reductions of carboxylate groups to corresponding alcohols (Gahloth et al., 2017), suggesting that engineered CARs might be able to directly reduce succinic acid to 1,4-BDO (Fig. 1). The objective of the present study was to use protein engineering to enhance MAB4714 activity toward succinate for the production of 1,4-BDO in combination with aldo-keto reductases (Fig. 1, the left pathway). We performed structural analysis (modeling) of MAB4714 to explore the feasibility of minimizing the carboxylate-binding pocket of this enzyme in order to increase its activity toward succinic acid. Using site-directed mutagenesis, we generated 16 MAB4714 mutant variants, and identified two variants with enhanced reductase activity toward succinic acid. We also investigated stability of purified CARs and the effect of protein expression conditions on CAR activity.

2. Materials and methods

2.1. Gene Cloning and Protein Purification

The genes encoding carboxylic acid reductases MAB4714 (Uniprot ID B1MLD7) and MSM5586 (Uniprot ID I7GER2) were amplified using PCR from genomic DNA of *Mycobacterium abscessus* and *M. smegmatis*, respectively, and cloned into a modified p15TVLic vector (Novagen) encoding an N-terminal 6His-tag as described previously (Kuznetsova et al., 2006). The phosphopantetheinyl transferase (PPT) BSU03570 (Sfp) from *Bacillus subtilis* was cloned into a pCDFDuet plasmid (without affinity tags) for co-expression with CARs in *Escherichia coli*. All plasmids were transformed into the expression host *E. coli* BL21(DE3) Gold strain (Agilent). Cultures were grown at 37 °C

in 1 L cultures (on TB medium) to OD_{600} 0.7 – 1.0, and protein expression was induced by the addition of 0.4 mM IPTG followed by overnight incubation at 26 °C (Table 1). Recombinant proteins were purified to near homogeneity (>95%) using Ni-chelate affinity chromatography on Ni-NTA Superflow resin (Qiagen) using standard protocols. Protein purity was analyzed using electrophoresis in 10% SDS polyacrylamide gels (SDS-PAGE). Site-directed mutagenesis of MAB4714 and MSM5586 was performed using the QuikChange™ site-directed mutagenesis kit (Stratagene) according to the manufacturer's protocol, and mutations were verified by DNA sequencing.

2.2. Enzymatic Assays

Carboxylate reductase activity against different carboxylic acids was determined spectrophotometrically using an NADPH oxidation-based assay by following the decrease in absorbance at 340 nm (ε_{340} = 6.22 $mM^{-1}\times cm^{-1}$) using a SpectraMax M2 plate-reader (triplicate assays in 96-well plates). CAR activity assays were performed at 30 °C in a reaction mixture (0.2 ml) containing 100 mM HEPES-K buffer (pH 7.5), 2 mM NADPH, 2.5 mM ATP, 10 mM $MgCl_2$, substrate (10 mM for aliphaticS acids, 2 mM cinnamic acid, or 100 mM succinic acid), and 5-10 µg of purified enzymes. The kinetics of MAB4714 were determined from specific activities over a range of substrate concentrations using 5-100 µg of purified proteins. The kinetic parameters (K_m and k_{cat}) were calculated by nonlinear regression analysis of raw data fit from Lineweaver-Burk plots using GraphPad Prism software (version 5.00 for Windows, GraphPad Software, San Diego, CA).

2.3. CAR Stability Assays

Protein stability of purified CARs (MSM5586 wild type and S713A mutant proteins) was analyzed using SDS-PAGE after incubation in the presence of different compounds (2 mM): ATP, ADP, CTP, polyphosphate, cinnamic acid, cinnamaldehyde, NADP, or NADPH. CAR samples (1.4 mg/ml) were incubated in 20 mM HEPES-K buffer (pH 7.5) containing 200 mM NaCl at room temperature for 30 h, and protein aliquots (5 µg) were analyzed using SDS-PAGE (10%). Effect of different compounds (Table 2) on stability of purified CAR was determined using MAB4714 (1 mg/ml) in 100 mM HEPES-K buffer (pH 7.5). After 16 h of incubation at 30 °C, the remaining CAR activity was measured in a reaction mixture containing 100 mM HEPES-K (pH 7.5), 5 mM benzoic acid, 10 mM $MgCl_2$, 1.5 mM ATP, and 0.4 mM NADPH.

2.4. Bioinformatics and Protein Modeling

Multiple sequence alignments of CARs were generated using the MAFFT online service (Katoh et al., 2017) and STRAP tool (Gille et al., 2014). Structural models of the MAB4714 A-domain were generated using the Phyre 2 web portal for protein modeling (Kelley et al., 2015). The MAB4714 models were built based on the recently determined crystal structures of the *Segnilliparus rugosus* CAR (*Sr*CAR, PDB codes 5MST and 5MSS, confidence 100%, sequence identity 59%). The substrate binding pockets of CARs was analyzed using PyMol version 2.4.

3. Results and discussion

3.1. Stability and activity of purified MAB4714

Enzyme stability is of paramount importance in many biocatalytic processes (Littlechild, 2015; Lorenz and Eck, 2005). CARs are large proteins with two separate domains connected by a flexible linker (Fig. 2), but their stability is not well understood. The previous work with *M. marinum* CAR suggested that it is a relatively stable enzyme, with *in vitro* half-life of 48 h at 37 °C (Akhtar et al., 2013). However, the recent study with five different CARs revealed a broad range of stability, with half-life at 30 °C ranging from 25 h to 123 h depending on the organism (Finnigan et al., 2017). In this work, we found that purified MAB4714 lost most of its catalytic activity after overnight storage at 4 °C (data not shown). Flash freezing in liquid nitrogen and subsequent storage at -80 °C reduced MAB4714 activity by ~30% (Table 1), but the frozen sample retained the remaining activity for several weeks (data not shown). We also determined the effect of different chemicals on stability of purified MAB4714 at 30 °C. After 16 hours of incubation at 30 °C, the control sample (no additions) retained 88% of initial activity indicating that MAB4714 is more stable at this temperature than at 4 °C (Table 2). The addition of DMSO, divalent cations (Ca^{2+}, Mg^{2+}), and diols (1,4-butanediol, 1,6-hexanediol) had destabilizing effects on MAB4714, with remaining activity 53-71%. Moderate stabilizing effects were observed in the presence of 10 mM polyphosphate (91.5% remaining activity), 10% glycerol (94%), and 150 mM NaCl (97%) (Table 2).

Recombinant expression of microbial CARs is not a trivial task, because these large proteins (over 1,000 amino acids) require post-translational modification via phosphopantetheinylation by a co-expressed phosphopantetheinyl transferase (PPT). Most published studies used the *Bacillus subtilis* BSU03570 (Sfp) for activation of recombinant CARs (Akhtar et al., 2013; Finnigan et al., 2017; Gahloth et al., 2017).

Indeed, our recent work demonstrated that this PPT enzyme produced slightly better results than the *E. coli* EntD when co-expressed with different CARs (Khusnutdinova et al., 2017). The optimal conditions for recombinant expression of *Mycobacterium phlei* CAR (*Mp*CAR) in *E. coli* cells have been determined as induction with 0.15 mM IPTG at OD_{600} = 0.6 followed by incubation (~18 h) at 20 °C (Finnigan et al., 2017). Similar expression conditions were found to be suitable for the recombinant expression of CARs from other organisms (Finnigan et al., 2017). In addition, several CARs were successfully produced using the auto-induction protocol described by Studier, which is based on the induction of protein expression by lactose (instead of IPTG) (Stolterfoht et al., 2017; Studier, 2005). The optimized protocol for recombinant expression and affinity purification of proteins from different organisms in *E. coli* developed by structural genomics projects includes growing *E. coli* cells at 37 °C to OD_{600} = 0.6 – 1.0 followed by IPTG induction (0.2 – 1.0 mM) and overnight incubation of cultures at 15 - 25 °C (Structural Genomics et al., 2008). It has been proposed that lower incubation temperatures facilitate proper fording of recombinant proteins during induction (Structural Genomics et al., 2008). In our standard protocol for recombinant protein expression and purification, the overnight incubation temperature is shifted to 16 °C (from 37 °C) after IPTG induction (Kuznetsova et al., 2006). When applied to MAB4714, this method produced 5-30 mg of purified enzyme (from 1 L cultures) with specific activities 0.4-0.6 U/mg (Table 1). Since this method produced large batch variations, we compared it with two modified protocols with higher induction temperatures (26 °C and 37 °C) and shorter incubation times (12 h and 5 h, respectively). As shown in Table 1, induction at 37 °C for 5 h resulted in reduced overall protein yield (6-7 mg), but had no

effect on CAR activity, whereas induction at 26 °C for 12 h produced more active MAB4714 (~1 U/mg) with more reproducible protein yields (12-18 mg). Therefore, this protocol was used for recombinant expression and purification of CARs.

3.2. Analysis of the substrate-binding site of MAB4714

Both *Sr*CAR and MAB4714 belong to sub-group II of bacterial CARs (Khusnutdinova et al., 2017), and share 61.5 % sequence identity at the amino acid level. Sequence analysis of microbial CARs revealed over 300 conserved residues with up to 160 residues in their A-domains (including the AMP-binding motif YTSGSTGxPKG), 25 residues in the PCP domain, and 170 in the R-domain (Finnigan et al., 2017; Stolterfoht et al., 2017; Stolterfoht et al., 2018) (Fig. 2A). Previous biochemical studies and crystal structures of CARs suggested that A domains (Fig. 2A) play a major role in substrate recognition by these enzymes (Finnigan et al., 2017; Gahloth et al., 2017; Stolterfoht et al., 2018; Wang and Zhao, 2014). Recent mutational studies with the *Neurospora crassa* CAR (*Nc*CAR) identified several amino acid residues of the A-domain critical for catalytic activity, including His237, Glu337, and Glu433, whereas alanine replacement mutations of Thr336, Asp405, and Arg422 resulted in a strong decrease in activity (Stolterfoht et al., 2017; Stolterfoht et al., 2018). However, the latter three residues appear to be not conserved in bacterial CARs, which share rather low sequence similarity with fungal CARs (~25% sequence identity). Nevertheless, the *Nc*CAR His237 is homologous to His315 in *Sr*CAR and His300 in *Ni*CAR, which are positioned close to both the AMP phosphate and the substrate carboxylate (Gahloth et al., 2017). Crystal structures of A-

domains in complex with AMP and acid substrates (benzoic acid or fumarate) revealed the relatively narrow substrate binding pocket lined by hydrophobic residues with the catalytic His (His300 in *Ni*CAR and His315 in *Sr*CAR) located at the bottom (Gahloth et al., 2017). The substrate binding pockets of *Sr*CAR and *Ni*CAR have different volumes and shapes, suggesting some differences in substrate preference of these CARs.

Using the Phyre2 web portal for protein modeling (Kelley et al., 2015), we generated a high quality structural model of MAB4714 (A-domain), which is based on the crystal structure of *Sr*CAR in complex with AMP and fumarate (PDB code 5MST; confidence 100%, 640 amino acids, 59% sequence identity) (Fig. 3). The model of the MAB4714 A-domain revealed a potential carboxylate-binding pocket located near the conserved His301 (His315 in *Sr*CAR) (Fig. 3). This pocket accommodates mostly hydrophobic residues, including Leu284, Thr285, Ala303, Leu306, Leu342, which might be involved in substrate recognition and binding (Fig. 3). In addition, there are at least five Gly residues in the MAB4714 substrate-binding pocket (Gly393, Gly395, Gly418, Gly420, Gly426), with three of them also conserved in *Sr*CAR (Gly405, Gly407, Gly432) (Fig. 3). In the MAB4714 sequence, these residues are located within the A_{core} domain, between the AMP-binding motif and the A_{sub} domain (Fig. 2A). A recent computational analysis of the *Sr*CAR structure suggested that conserved Thr265 (Thr258 in MAB4714), Ser408 (Ser396 in MAB4714), and Thr505 (Thr493 in MAB4714) might play an important role in substrate recognition (Qu et al., 2019). In the MAB4714 A-domain model, Thr258 and Thr493 are positioned outside of the carboxylate-binding pocket, whereas Ser396 is located at the bottom of the carboxylate-binding pocket near the conserved His301, suggesting that it might contribute to substrate binding.

We hypothesized that binding of succinic acid in the MAB4714 active site might be facilitated by the reduction of the volume of carboxylate-binding pocket, e.g. by replacing small residues or glycines with larger side chains (hydrophobic or non-polar). Based on the MAB4714 structural model (Fig. 4), we selected nine residues (hydrophobic, polar, or Gly) located near the distal (to His301) end of the pocket and mutated them to larger hydrophobic residues (Trp, Phe, Leu) using site-directed mutagenesis. As controls, we also introduced polar (Gln) or negatively charged (Glu) residues to several positions. Sixteen clones produced soluble mutant proteins, which were affinity purified and assayed for carboxylate reductase activity with cinnamic acid and succinic acid as substrates (Fig. 5).

3.3. Carboxylate reductase activity of MAB4714 mutant proteins

For purified wild type MAB4714, carboxylate reductase activity against cinnamic acid was approximately 500 times higher than that toward succinic acid (Fig. 5). The replacement of Gly420 with Trp or Glu completely abolished reductase activity of MAB4714 against cinnamic acid. With succinic acid as substrate, G420W retained wild-type activity, whereas the activity of G420E was two times lower (Fig. 5). This suggests that the introduction of a bulky side chain at the position of Gly420 prevents binding of aromatic substrates in the MAB4714 active site but has minor effects on succinic acid binding. Cinnamic acid reductase activity was unaffected in the MAB4714 mutant proteins T285E, A303L, L306W, L342F, L342E, L342Q, G395E, and G426W, slightly reduced in T285W, A303E, and G418E, and reduced by 50% in L284W, G393W, and

G395L (Fig. 5). In *Nc*CAR, alanine replacement of Lys190 and Pro234 increased its reductase activity toward cinnamic acid (Stolterfoht et al., 2017). However, none of the MAB4714 mutant proteins obtained in this work showed increased activity with cinnamic acid (Fig. 5).

With succinic acid as substrate, most MAB4714 mutant proteins showed reduced reductase activity, including A303L, A303E, L306W, L342F, L342E, G395L, G395E, G418E, G420W, and G420E, while G426W had wild-type activity (Fig. 5). In the MAB4714 A-domain structural model, these residues are located at the bottom or middle of carboxylate-binding pocket, near the catalytic His301 (4 – 13 Å) (Fig. 4). This area seems to be more critical for succinate binding compared to cinnamic acid (except for Gly420). However, succinate reductase activity was increased by ~ 50% in T285E and L342Q proteins, whereas L284W and T285W were found to be at least two times more active than wild type MAB4714 (although the reaction rates remain low) (Fig. 5).

Analysis of kinetic parameters of L284W and T285W with cinnamic acid as a substrate revealed that they had lower K_m values compared to the wild-type MAB4714, but their k_{cat} were similar (for T285W) or lower (for L284W) (Table 3). With succinic acid as substrate, we were unable to get accurate determinations for wild-type MAB4714, but the observed k_{cat} values for L284W and T285W (0.16-0.20 s^{-1}) were approximately two times higher than that reported for MarCAR and MavCAR (Kramer et al., 2018). However, the affinity of both L284W and T285W to succinic acid was at least three orders of magnitude lower than to cinnamic acid indicating that more work is required to improve binding of succinic acid (Table 3).

As shown in Fig. 5, replacement of Leu284 and Thr285 by Trp (Fig. 4) had positive effects on the MAB4714 activity against succinic acid. The results suggest that these mutations appear to reduce the volume of carboxylate-binding pocket facilitating binding of succinic acid. This is in line with the side chain orientation of the homologous Ala293 and Phe294 (Leu284 and Thr285 in MAB4714, respectively) in the structure of the *Sr*CAR-fumarate complex (PDB code 5MST, Fig. 3B). In bacterial CARs, these residues are located on a flexible loop of variable length (9-14 aa) connecting the α helix-14 and β strand-10 in the *Sr*CAR structure (PDB code 5MSS) and accommodating mostly non-conserved residues (Fig. 2). In a recent study with *Nc*CAR, replacement of Pro234 or Pro285 by Ala elevated the activity of this enzyme against longer aliphatic acids, probably due to the increased flexibility of the associated secondary structures (Stolterfoht et al., 2018). Based on the MAB4714 A-domain structural model, the carboxylate-binding pocket contains the highly conserved Pro290 (located on the Leu284-Thr285 loop) and conserved Pro298 (located near the catalytic His301) (Fig. 2). These Pro residues, as well as the residues of the Leu284-Thr285 loop and near Leu342 (and their combinations) represent attractive targets for future protein engineering studies on MAB4714.

3.4. Role of CAR phosphopantetheinylation in protein stability

Covalent modification of CARs via phosphopantetheinylation has been shown to be necessary for catalytic activity of these enzymes (Venkitasubramanian et al., 2007). Surprisingly, we found that CAR phosphopantetheinylation is also important for their

stability. In preliminary crystallization studies with different CARs (including MAB4714), we were able to crystallize the CAR enzyme MSM5586 (A domain) from *Mycobacterium smegmatis* (but not MAB4714). In order to improve crystal quality, we generated the S713A mutant variant of MSM5586 to produce a more uniform protein preparation containing only unmodified CAR molecules. This Ser residue is conserved in all CARs and represents the attachment site for the phosphopantetheinyl arm involved in the transfer of catalytic intermediate from A-domain to R-domain (Gahloth et al., 2017). As shown in Fig. 6, freshly purified MSM5586 S713A variant had electrophoretic mobility on 10% SDS-gels similar to that of the wild-type protein, producing one major band with apparent M_r 130 kDa (calculated M_r 129.9 kDa). After 30 hours of incubation at room temperature, the wild-type MSM5586 showed no visible protein degradation (Fig. 6). In contrast, purified S713A mutant protein was almost completely degraded, with the formation of two major products of apparent M_r 75 kDa and 55 kDa (Fig. 6). Molecular masses of these products suggest that the MSM5586 polypeptide chain was broken within the PCP domain near Ser713 producing the separate A-domain (~ 1-712 aa, calculated M_r 77.1 kDa) and R-domain (~ 713-1,193 aa, calculated M_r 52.8 kDa). Addition of ATP or CTP had moderate stabilizing effects on S713A, whereas other additions (ADP, AMP, pyrophosphate, cinnamic acid, cinnamaldehyde, NADPH) had no effect. Addition of NADP to purified S713A resulted in strong protein precipitation, and SDS-PAGE showed no apparent MSM5586 degradation (Fig. 6), suggesting that precipitated S713A is more stable than that in solution. All tested compounds had no effect on the stability of wild type MSM5586 (Fig. 6A). These results suggest that phosphopantetheinylation of CARs prevents fast degradation of purified proteins in

solution (and probably *in vivo* in *E. coli* cells). Thus, the presence of phosphopantetheinyl group in CARs seems to be essential for stability of these enzymes *in vitro*.

4. Conclusions

In this work, we performed structural analysis of the carboxylate binding pocket of MAB4714 and suggested that its activity toward succinic acid can be increased by reducing the pocket volume. Using site-directed mutagenesis, we introduced larger side chains to various positions of the MAB4714 carboxylate-binding pocket and determined catalytic activity of purified mutant proteins against cinnamic acid and succinic acid. We found that, although the reaction rates remain low, the replacement of Leu284 and Thr285 with Trp increased reductase activity of MAB4714 toward succinic acid more than two times. These results suggest that this locus and potentially other residues on this strand (Lys281 – Ser291) represent attractive targets for future protein engineering studies toward enhanced activity of CARs against succinic acid. We also demonstrated that phosphopantetheinylation of CARs is important for stability of purified proteins in solution, which can also be stabilized by the addition of NaCl, polyphosphate, and glycerol. The obtained MAB4714 variants can be used as starting material for future protein engineering efforts aimed at improving the activity of CARs against succinic acid for the biotechnological production of 1,4-BDO and other chemicals.

Declaration of interests

None

Acknowledgements

This work was supported by the Natural Sciences and Engineering Research Council (NSERC) Strategic Network grant IBN, Ontario Research Fund (ORF Reserch Excellence) grant BioCeB (Biochemicals from Cellulosic Biomass), and a grant from the Genome Canada, Genomics Applied Partnership Program (GAPP).

References

Akhtar, M.K., Turner, N.J., Jones, P.R., (2013) Carboxylic acid reductase is a versatile enzyme for the conversion of fatty acids into fuels and chemical commodities. Proc Natl Acad Sci U S A 110, 87-92.
Alonso, S., Rendueles, M., Diaz, M., (2015) Microbial production of specialty organic acids from renewable and waste materials. Crit Rev Biotechnol 35, 497-513.
Bornscheuer, U.T., Huisman, G.W., Kazlauskas, R.J., Lutz, S., Moore, J.C., Robins, K., (2012) Engineering the third wave of biocatalysis. Nature 485, 185-194.
Bozell, J.J., and Petersen, G.R., (2010) Technology development for the production of biobased products from biorefinery carbohydrates - the US Department of Energy's "Top 10" revisited. Green Chem. 12, 539-554.
Finnigan, W., Thomas, A., Cromar, H., Gough, B., Snajdrova, R., Adams, J.P., Littlechild, J.A., Harmer, N.J., (2017) Characterization of Carboxylic Acid Reductases as Enzymes in the Toolbox for Synthetic Chemistry. ChemCatChem 9, 1005-1017.
Gahloth, D., Dunstan, M.S., Quaglia, D., Klumbys, E., Lockhart-Cairns, M.P., Hill, A.M., Derrington, S.R., Scrutton, N.S., Turner, N.J., Leys, D., (2017) Structures of carboxylic acid reductase reveal domain dynamics underlying catalysis. Nat Chem Biol 13, 975-981.
Gille, C., Fahling, M., Weyand, B., Wieland, T., Gille, A., (2014) Alignment-Annotator web server: rendering and annotating sequence alignments. Nucleic Acids Res 42, W3-6.
Gross, G.G., (1969) Evidence for enzyme-substrate intermediates in the aryl-aldehyde: NADP oxidoreductase catalysed reduction of salicylate. FEBS Lett 5, 177-179.
He, A., Li, T., Daniels, L., Fotheringham, I., Rosazza, J.P., (2004) Nocardia sp. carboxylic acid reductase: cloning, expression, and characterization of a new aldehyde oxidoreductase family. Appl Environ Microbiol 70, 1874-1881.
Hollmann, F., Arends, I.W.C.E., and Holtmann, D., (2011) Enzymatic reductions for the chemist. Green Chem. 13, 2285-2313.
Jang, Y.S., Kim, B., Shin, J.H., Choi, Y.J., Choi, S., Song, C.W., Lee, J., Park, H.G., Lee, S.Y., (2012) Bio-based production of C2-C6 platform chemicals. Biotechnol Bioeng 109, 2437-2459.
Kallio, P., Pasztor, A., Thiel, K., Akhtar, M.K., Jones, P.R., (2014) An engineered pathway for the biosynthesis of renewable propane. Nat Commun 5, 4731.
Katoh, K., Rozewicki, J., Yamada, K.D., (2017) MAFFT online service: multiple sequence alignment, interactive sequence choice and visualization. Brief Bioinform bbx108, 1-7.
Kelley, L.A., Mezulis, S., Yates, C.M., Wass, M.N., Sternberg, M.J., (2015) The Phyre2 web portal for protein modeling, prediction and analysis. Nat Protoc 10, 845-858.
Khusnutdinova, A.N., Flick, R., Popovic, A., Brown, G., Tchigvintsev, A., Nocek, B., Correia, K., Joo, J.C., Mahadevan, R., Yakunin, A.F., (2017) Exploring Bacterial Carboxylate Reductases for the Reduction of Bifunctional Carboxylic Acids. Biotechnol J 12, 1600751.

Kramer, L., Hankore, E.D., Liu, Y., Liu, K., Jimenez, E., Guo, J., Niu, W., (2018) Characterization of Carboxylic Acid Reductases for Biocatalytic Synthesis of Industrial Chemicals. Chembiochem 19, 1452-1460.
Kunjapur, A.M., Tarasova, Y., Prather, K.L., (2014) Synthesis and accumulation of aromatic aldehydes in an engineered strain of Escherichia coli. J Am Chem Soc 136, 11644-11654.
Kuznetsova, E., Proudfoot, M., Gonzalez, C.F., Brown, G., Omelchenko, M.V., Borozan, I., Carmel, L., Wolf, Y.I., Mori, H., Savchenko, A.V., Arrowsmith, C.H., Koonin, E.V., Edwards, A.M., Yakunin, A.F., (2006) Genome-wide analysis of substrate specificities of the Escherichia coli haloacid dehalogenase-like phosphatase family. J Biol Chem 281, 36149-36161.
Li, T., Rosazza, J.P., (1997) Purification, characterization, and properties of an aryl aldehyde oxidoreductase from Nocardia sp. strain NRRL 5646. J Bacteriol 179, 3482-3487.
Li, T., Rosazza, J.P., (1998) NMR identification of an acyl-adenylate intermediate in the aryl-aldehyde oxidoreductase catalyzed reaction. J Biol Chem 273, 34230-34233.
Littlechild, J.A., (2015) Enzymes from Extreme Environments and Their Industrial Applications. Front Bioeng Biotechnol 3, 161.
Lorenz, P., Eck, J., (2005) Metagenomics and industrial applications. Nat Rev Microbiol 3, 510-516.
Napora-Wijata, K., Strohmeier, G.A., Winkler, M., (2014) Biocatalytic reduction of carboxylic acids. Biotechnol J 9, 822-843.
Qu, G., Fu, M., Zhao, L., Liu, B., Liu, P., Fan, W., Ma, J.A., Sun, Z., (2019) Computational Insights into the Catalytic Mechanism of Bacterial Carboxylic Acid Reductase. J Chem Inf Model 59, 832-841.
Schwendenwein, D., Fiume, G., Weber, H., Rudroff, F., Winkler, M., (2016) Selective Enzymatic Transformation to Aldehydes in vivo by Fungal Carboxylate Reductase from Neurospora crassa. Adv Synth Catal 358, 3414-3421.
Sheppard, M.J., Kunjapur, A.M., Prather, K.L.J., (2016) Modular and selective biosynthesis of gasoline-range alkanes. Metab Eng 33, 28-40.
Sheppard, M.J., Kunjapur, A.M., Wenck, S.J., Prather, K.L., (2014) Retro-biosynthetic screening of a modular pathway design achieves selective route for microbial synthesis of 4-methyl-pentanol. Nat Commun 5, 5031.
Stolterfoht, H., Schwendenwein, D., Sensen, C.W., Rudroff, F., Winkler, M., (2017) Four distinct types of E.C. 1.2.1.30 enzymes can catalyze the reduction of carboxylic acids to aldehydes. J Biotechnol 257, 222-232.
Stolterfoht, H., Steinkellner, G., Schwendenwein, D., Pavkov-Keller, T., Gruber, K., Winkler, M., (2018) Identification of Key Residues for Enzymatic Carboxylate Reduction. Front Microbiol 9, 250.
Structural Genomics, C., China Structural Genomics, C., Northeast Structural Genomics, C., Graslund, S., Nordlund, P., Weigelt, J., Hallberg, B.M., Bray, J., Gileadi, O., Knapp, S., Oppermann, U., Arrowsmith, C., Hui, R., Ming, J., dhe-Paganon, S., Park, H.W., Savchenko, A., Yee, A., Edwards, A., Vincentelli, R., Cambillau, C., Kim, R., Kim, S.H., Rao, Z., Shi, Y., Terwilliger, T.C., Kim, C.Y., Hung, L.W., Waldo, G.S., Peleg, Y., Albeck, S., Unger, T., Dym, O., Prilusky, J., Sussman, J.L., Stevens, R.C., Lesley, S.A., Wilson, I.A., Joachimiak, A., Collart, F., Dementieva, I., Donnelly, M.I., Eschenfeldt,

W.H., Kim, Y., Stols, L., Wu, R., Zhou, M., Burley, S.K., Emtage, J.S., Sauder, J.M., Thompson, D., Bain, K., Luz, J., Gheyi, T., Zhang, F., Atwell, S., Almo, S.C., Bonanno, J.B., Fiser, A., Swaminathan, S., Studier, F.W., Chance, M.R., Sali, A., Acton, T.B., Xiao, R., Zhao, L., Ma, L.C., Hunt, J.F., Tong, L., Cunningham, K., Inouye, M., Anderson, S., Janjua, H., Shastry, R., Ho, C.K., Wang, D., Wang, H., Jiang, M., Montelione, G.T., Stuart, D.I., Owens, R.J., Daenke, S., Schutz, A., Heinemann, U., Yokoyama, S., Bussow, K., Gunsalus, K.C., (2008) Protein production and purification. Nat Methods 5, 135-146.
Studier, F.W., (2005) Protein production by auto-induction in high density shaking cultures. Protein Expr Purif 41, 207-234.
Venkitasubramanian, P., Daniels, L., Rosazza, J.P., (2007) Reduction of carboxylic acids by Nocardia aldehyde oxidoreductase requires a phosphopantetheinylated enzyme. J Biol Chem 282, 478-485.
Wang, M., Zhao, H., (2014) Characterization and Engineering of the Adenylation Domain of a NRPS-Like Protein: A Potential Biocatalyst for Aldehyde Generation. ACS Catal 4, 1219-1225.
Winkler, M., (2018) Carboxylic acid reductase enzymes (CARs). Curr Opin Chem Biol 43, 23-29.
Yim, H., Haselbeck, R., Niu, W., Pujol-Baxley, C., Burgard, A., Boldt, J., Khandurina, J., Trawick, J.D., Osterhout, R.E., Stephen, R., Estadilla, J., Teisan, S., Schreyer, H.B., Andrae, S., Yang, T.H., Lee, S.Y., Burk, M.J., Van Dien, S., (2011) Metabolic engineering of Escherichia coli for direct production of 1,4-butanediol. Nat Chem Biol 7, 445-452.

Figure legends

Fig. 1. The biocatalytic conversion of succinate to 1,4-BDO. Schematic diagram showing enzymatic reactions for the biotransformation of succinate to 1,4-BDO. The right part shows the reactions constituting the engineered pathway for 1,4-BDO biosynthesis from succinate demonstrated by Yim et al. (Yim et al., 2011). The numbered steps represent the following enzymes: (1), succinyl-CoA synthetase; (2), CoA-dependent succinate semialdehyde dehydrogenase; (3), 4-hydroxybutyrate dehydrogenase; (4), 4-hydroxybutyryl-CoA transferase; (5), 4-hydroxybutyryl-CoA reductase; (6), alcohol dehydrogenase. The other biochemical reactions involve CAR and AKR (aldo-keto reductase).

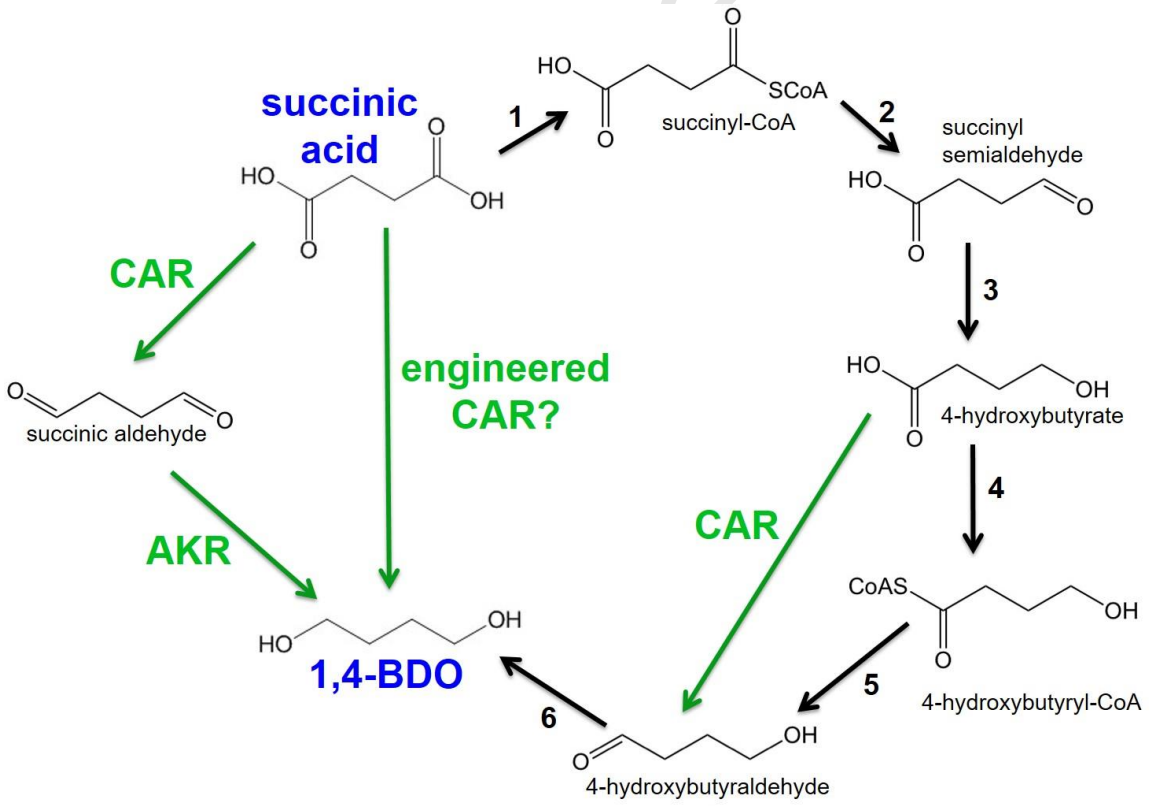

Fig. 2. Domain organization of MAB4714 and sequence alignment of CAR A-domains. (A), Domain organization of MAB4714. Adenylation domain (A-domain core and A-sub-domain), PCP (peptidyl carrier protein domain, phosphopantetheine attachment site), reductase domain (R-domain). Domain boundaries are indicated by residue numbers (above the diagram). (B), Sequence alignment of A-domains of MAB4714 and four other CARs. Conserved residues are shown in bold, whereas the AMP-binding motif is colored orange. The MAB4714 residues mutated in this work are shown in red and numbered, and the residues from the *Sr*CAR substrate binding site are colored blue and numbered. The sequence alignment includes the following CARs: *Sr*CAR (*S. rugosus*, Uniprot ID E5XP76), *Ni*CAR (*N. iowensis*, Q6RKB1), MCH22995 (*M. chelonae*, A0A0E3TT64), MSM5586 (*M. smegmatis*, I7GER2), and MAB4714 (*M. abscessus*, B1MLD7).

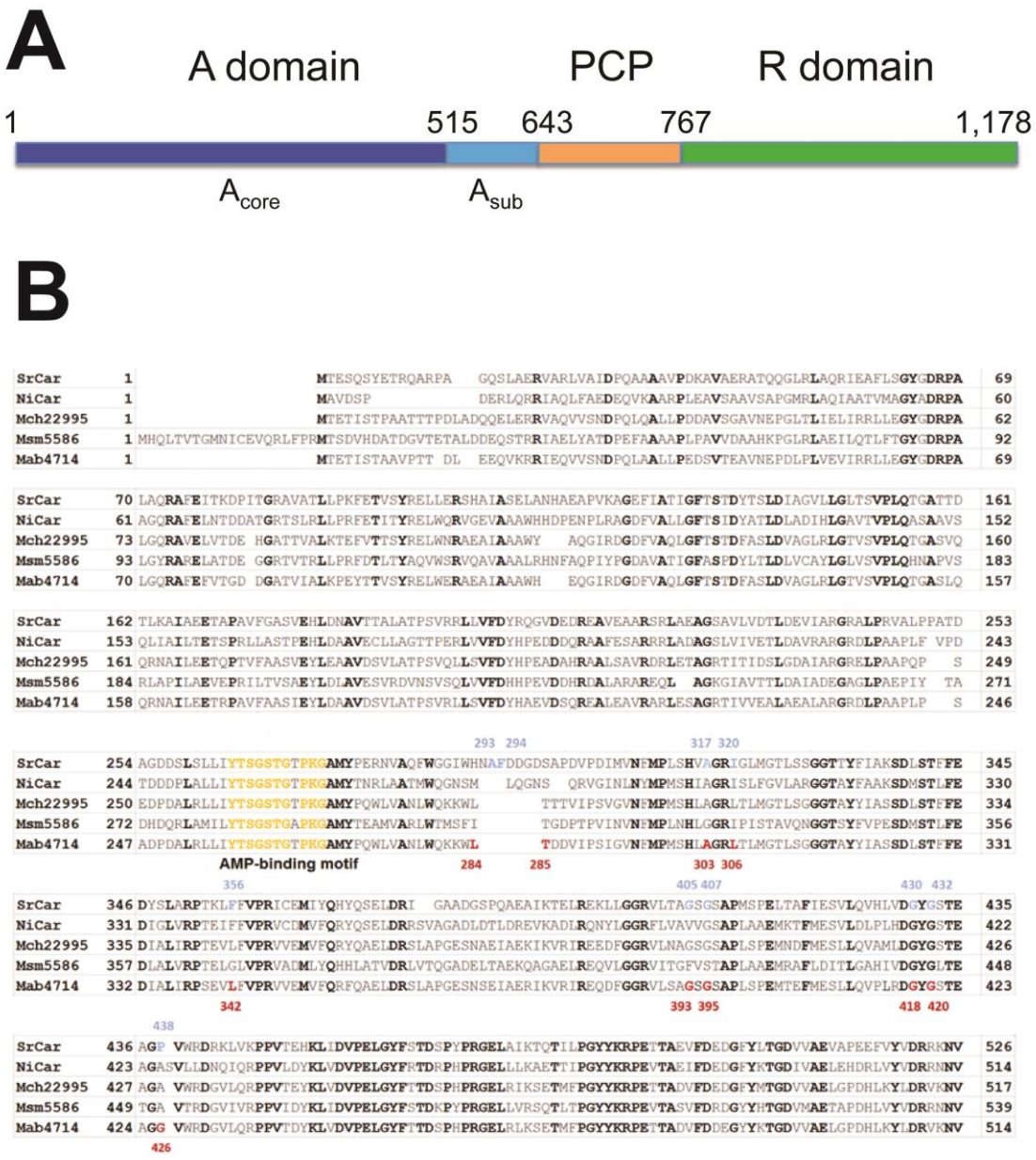

Fig. 3. Structural analysis of the CAR carboxylate-binding pocket. (A), Crystal structure of the *S. rugosus* CAR (*Sr*CAR) A domain in complex with fumarate and AMP (PDB code 5MST) (Gahloth et al., 2017). The overall fold of domain is shown in semi-transparent surface representation to reveal the bound ligands and secondary structural elements. (B), Close-up view of the substrate-binding pocket showing bound AMP and fumarate. Ligand molecules are shown as sticks with yellow (AMP) or green (fumarate)

carbons, whereas side chains of *Sr*CAR are shown as sticks with brown carbons and labeled. The black labels indicate the corresponding residues of MAB4714 identified based on sequence alignment with *Sr*CAR (Figure 2).

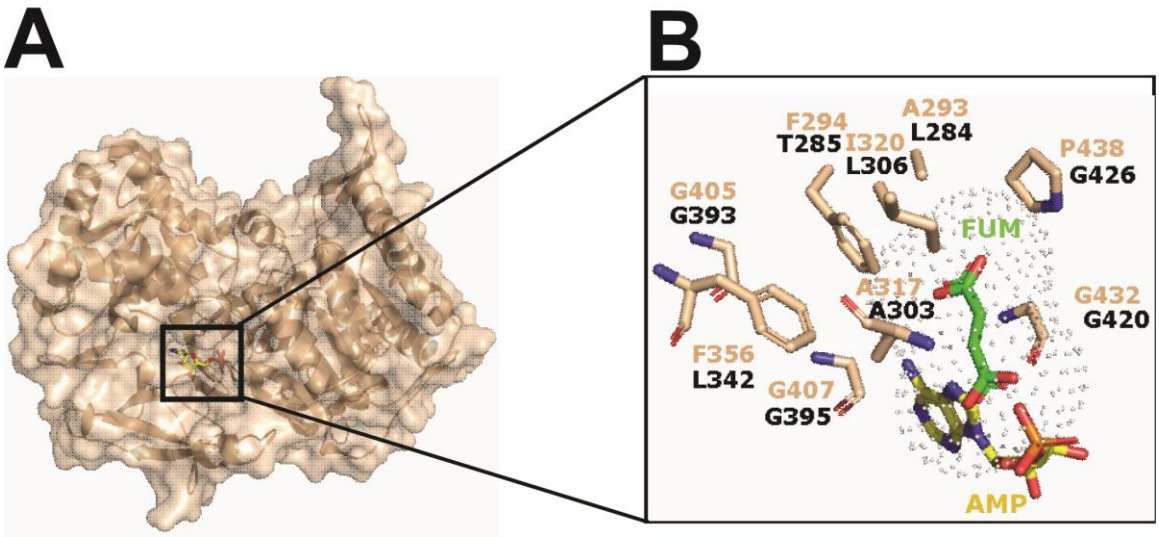

Fig. 4. Structural models of substrate-binding pocket of MAB4714. (A), Close-up view of the wild-type carboxylate-binding pocket showing catalytic His301 and residues mutated in this work. (B), Carboxylate-binding pocket of the L284W mutant protein. (C), Carboxylate-binding pocket of the T285W mutant protein. The MAB4714 structural model was generated using the Phyre2 portal (Kelley et al., 2015) and is based on the structure of *Sr*CAR (PDB code 5MSS, sequence identity 59%, confidence 100%). Protein ribbon diagrams are colored in gray, whereas side chains are shown as sticks with green carbons.

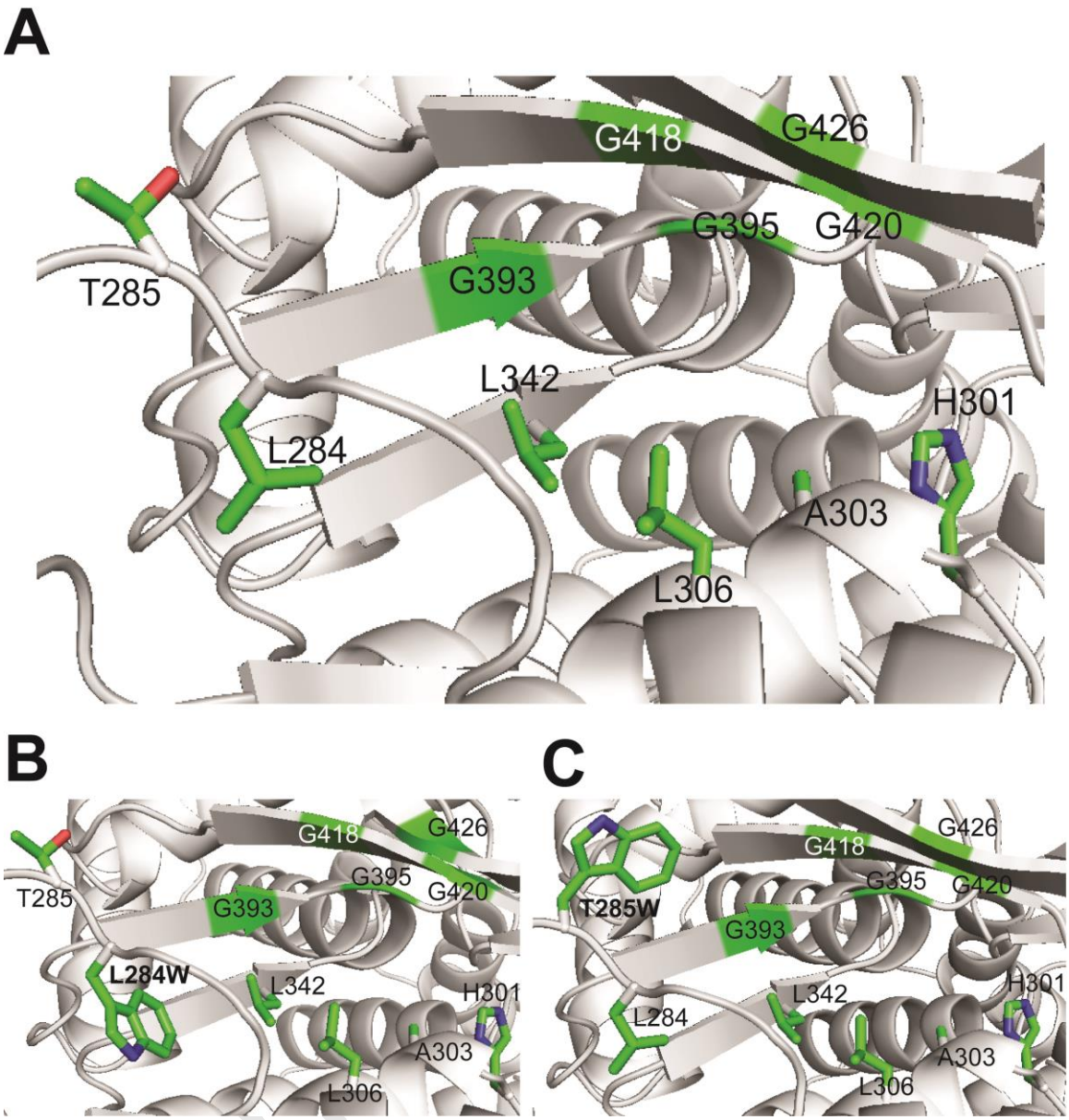

Fig. 5. Site-directed mutagenesis of MAB4714: carboxylate reductase activity of purified wild-type and mutant proteins. (A), Cinnamic acid as substrate. (B), Succinic acid as substrate. Enzyme activities were determined by following NADPH oxidation in a reaction mixture containing 100 mM HEPES-K buffer (pH 7.5), 0.5 mM NADPH, 2.5 mM ATP, 10 mM $MgCl_2$, 2 mM cinnamic acid (or 100 mM succinic acid), and 3-5 μg of purified MAB4714 protein.

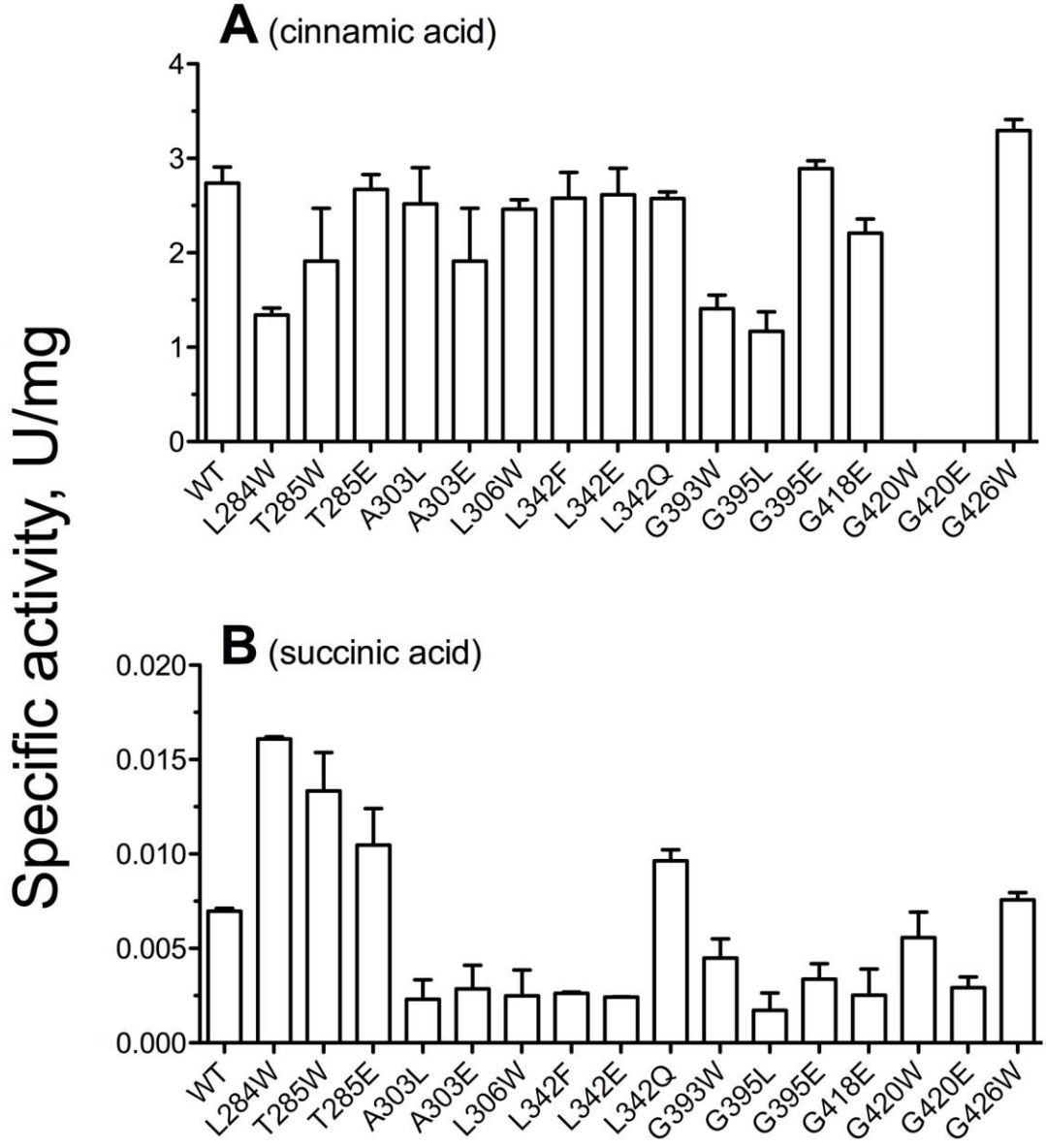

Fig. 6. Mutation of MSM5586 Ser713 to Ala reduces CAR stability in solution. Coomassie-stained SDS-gels showing purified wild-type (A) and S713A mutant (B) proteins after 30 h of incubation at room temperature. Molecular weight markers are shown on the left sides of gels, whereas apparent M_r of the two major degradation products are shown on the right side of B (75 kDa and 55 kDa).

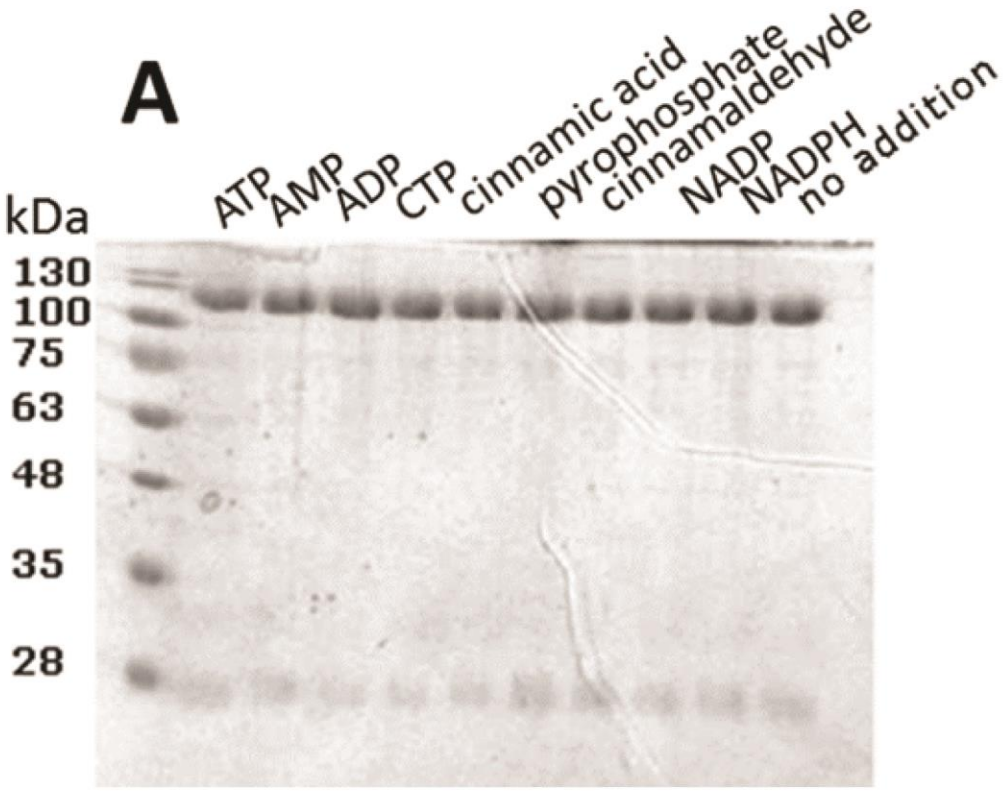
A
ATP
AMP
ADP
CTP
cinnamic acid
pyrophosphate
cinnamaldehyde
NADP
NADPH
no addition
kDa
130
100
75
63
48
35
28

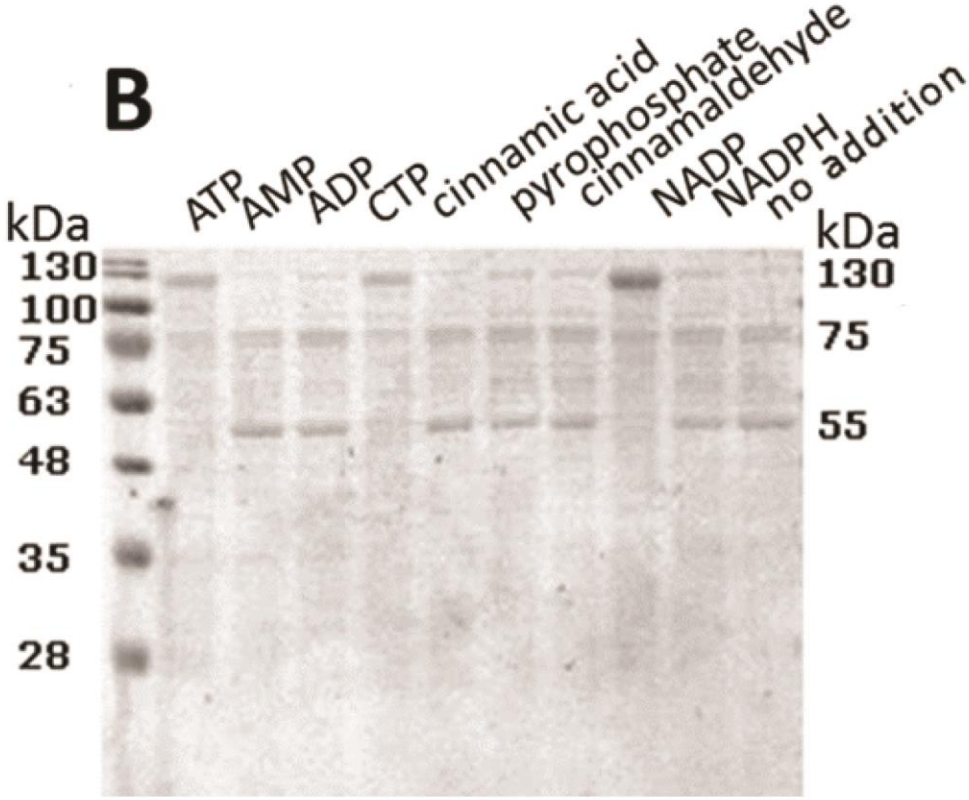
B
ATP
AMP
ADP
CTP
cinnamic acid
pyrophosphate
cinnamaldehyde
NADP
NADPH
no addition
kDa
130
100
75
63
48
35
28
kDa
130
75
55

Table

Table 1. Effect of protein storage and expression conditions on reductase activity of purified MAB4714 with cinnamic acid (2 mM) as substrate.

Protein storage conditions	**Activity, U/mg**
Control (initial activity)	1.56 ± 0.03
-80 °C, 1 day, no additions	1.05 ± 0.03
-80 °C, 1 day, 5 mM DTT	0.43 ± 0.02
-80 °C, 6 days, no additions	0.90 ± 0.03
Protein expression conditions (after IPTG addition)	
Incubation for 20 hours at 16 °C	0.53 ± 0.09 (16.4 ± 11.6)[a]
Incubation for 12 hours at 26 °C	1.05 ± 0.03 (15.5 ± 3.3)
Incubation for 5 hours at 37 °C	0.41 ± 0.05 (6.5 ± 1.2)

[a] Numbers in brackets indicate CAR protein yield (mg/L of *E. coli* culture).

Table 2. Stability of purified MAB4714: reductase activity after incubation with different compounds[a].

Compounds	**Concentration**	**Residual activity, %**
1. No addition	N/A[b]	88.1±2.3
2. $MgCl_2$	10 mM	73.9±8.1
3. $CaCl_2$	10 mM	53.3±1.5
4. EDTA	1 mM	82.6±19.0
5. DMSO	1 %	64.8±7.6
6. TCEP	0.5 mM	78.4±1.8
7. Citrate Na	50 mM	75.5±6.2
8. Formate Na	50 mM	66.9±2.7
9. Formate Na	100 mM	67.1±3.2
10. Polyphosphate	1 mM	72.7±3.0
11. Polyphosphate	5 mM	72.8±11.4
12. Polyphosphate	10 mM	91.5±5.2

13. Glycerol	10 %	93.9±2.8
14. NaCl	50 mM	92.3±3.5
15. NaCl	150 mM	97.3±6.3
16. NaCl	250 mM	89.6±1.1
17. NaCl	350 mM	84.8±1.0
18. NaCl	450 mM	82.5±4.7
19. KCl	50 mM	82.5±12.9
20. KCl	150 mM	86.2±6.7
21. KCl	250 mM	84.8±2.7
22. KCl	350 mM	88.5±4.8
23. KCl	450 mM	91.5±4.4
24. 1,4-butanediol	10 mM	62.0±4.7
25. 1,6-hexanediol	10 mM	71.2±6.4

[a] Purified MAB4714 (1 mg/ml) was incubated for 16 h at 30°C with indicated compounds, and residual reductase activity was measured using 5 mM benzoic acid as substrate (in 0.1 M Hepes-K, pH 7.5,10 mM $MgCl_2$, 1.5 mM ATP, 0.4 mM NADPH, at 30°C). Activities are presented as % of the initial activity before incubation with compounds (100% = 3.7 ± 0.1 U/mg).

[b] N/A, not applicable.

Table 3. Kinetic parameters of purified wild type and mutant MAB4714 proteins with cinnamic acid and succinic acid as substrates.

Variable substrate	**Protein**	K_m, **mM**	k_{cat}, s^{-1}	k_{cat}/K_m, $M^{-1}s^{-1}$
cinnamic acid	wild type	0.56 ± 0.07	1.95 ± 0.07	0.4×10^4
	L284W	0.35 ± 0.06	1.56 ± 0.02	0.5×10^4
	T285W	0.27 ± 0.03	2.07 ± 0.07	0.8×10^4
succinic acid	wild type	545 ± 166	0.12 ± 0.02	0.3
	L284W	161 ± 17	0.20 ± 0.01	0.1×10^1
	T285W	336 ± 34	0.16 ± 0.01	0.1×10^1